Fatigue behavior of 2618-T851 aluminum alloy under uniaxial and multiaxial loadings

Malek Benaïssa, Catherine Mabru, Michel Chaussumier

Fatigue behavior of 2618-T851 aluminum alloy under uniaxial and multiaxial loadings

Benaïssa Malek, Catherine Mabru, Michel Chaussumier*

Université de Toulouse, Institut Clément Ader (ICA), UMR CNRS 5312, UPS/INSA/ISAE/ Mines Albi, 3 Rue Caroline Aigle, 31400 Toulouse, France

Keywords:
AA2618-T851
Multiaxial fatigue
Roughness
Crossland criterion

A B S T R A C T

AA2618 aeronautical aluminum alloy has been largely used in the past, especially in well-known Concorde aircraft, developed during sixties decade. In more recent aircraft, this alloy has been largely replaced by others such as 7075 which present greater fatigue resistance. Forgotten for a time, AA2618 comes back in new aircrafts for structural parts submitted to fatigue loading at high temperature because of only a slight decrease of fatigue resistance of this alloy compared to room temperature fatigue resistance. In this paper, a complete fatigue characterization of 2618-T851 aluminum alloy is presented: fatigue tests under uniaxial tensile or torsion cyclic loadings, with mean tensile or shear stress have been realized; fatigue tests under combined tensile-torsion, in or out-of-phase have also been conducted as well as some combined tensile-torsion-internal pressure fatigue tests. All these tests covered 10^4–10^7 cycles range. At last, Crossland multiaxial fatigue criterion has been used and extended to median fatigue life domain to analyze these results.

1. Introduction

Derived from high strength aluminum alloys developed before first world war by Royce Rolls (RR serie 1929), aluminum copper 2618 T851 alloy (Hiduminium RR58; AU2GN) has been further developed by High Duty Alloys Ltd for aircraft gas turbine compressor engines and has been widely used in Concorde aircraft structure (fuselage skin, outer skin of engines, wings) because of its high resistance stress level, its low density and its high resistance at high temperature (130 °C) [1,2]. This aluminum alloy is an Al Cu Mg Fe Ni alloy; Fe and Ni atomic elements addition are responsible of this high temperature re sistance as they form coarse intermetallic particles (Al_9FeNi) providing microstructural stability at high temperature. Nowadays this alloy has been replaced by aluminum alloys such as 2214 or 7075. However, 2618 aluminum alloy is still used in industrial applications that involve high strength to weight ratio with high temperature exposures such as compressor wheels of exhaust turbochargers or automotive engine cy linder heads or aeronautical applications such as components of aircraft engines. This alloy can be also employed for application where short time exposure to temperature up to 300 °C is involved. Some research works have been recurrently realized in the four last decades con cerning this particular alloy; most of these research studies concern microstructural characterization and deal with the condition of for mation of intermetallic particles during heat treatment [3 8]. AA2618 T6 microstructure generally consists of mixed recrystallized and non recrystallized solid solution Al α Cu Mg grains, a slight proportion of stable S phase Al_2CuMg fine coherent plate like intermetallic pre cipitates homogeneously distributed in the matrix, and, in larger pro portion (99%), of stable Al_9FeNi intermetallic particles distributed in homogeneously in Al α grains as wells as in grains boundaries. S phase coarse particles can rarely appear in grain boundaries; in that case precipitates free zone (PFZ) are observed along grain boundaries. S phase particles are identified to mainly contribute to strengthening; it has been also shown that metastable S phase needles size was sensitive to deformation before ageing treatment; S phase needles are smaller in deformation ageing state, and consequently, dispersion strengthening is more efficient. Otherwise, hardness peak during ageing treatment is reached faster in DAT state than in T6 state. Moreover, Al_9FeNi are identified to contribute to grain size control at elevated temperature and dispersion hardening as effective barrier for dislocation movement. Other type of intermetallic particles (Al_2Cu, Mg_2Si, AlCuNi, Al_7Cu_2Fe) can be found also. As well as for all 2xxx, 6xxx or 7xxx aluminum al loys, monotonic mechanical properties (yield stress, ultimate strength and elongation) clearly depend on heat treatment conditions, especially on aging conditions even if the conditions of solution treatment have also unneglectable influence as it controls the dissolution of most of intermetallic particles in the matrix, except Al_9FeNi particles.

Since the first mechanical behavior investigation [9 11], AA2618

* Corresponding author.
E-mail address: michel.chaussumier@insa-toulouse.fr (M. Chaussumier).

https://doi.org/10.1016/j.ijfatigue.2019.105322

mechanical behavior has been largely investigated under monotonic tensile loading at room temperature [12,13] or under creep conditions [14 17]. However, only few papers deal with fatigue resistance. In the 70′ 80′, a French research consortium of 10 laboratories carried out a large experience plan to investigate fatigue crack propagation and fa tigue threshold in particular [18,19]; it has been concluded that stress ratio is the main parameter influencing fatigue threshold compared to other experimental parameters such as environment, temperature, fre quency, waveform and grain size. From these research results, Paris law parameters are available for three grain sizes (small, medium and large size). Fracture toughness values are also available in [20]. Recent re search works investigated uniaxial fatigue behavior at room and/or elevated temperatures [21 23] in order to understand the role of mi crostructure and particularly the role of intermetallic particles on fa tigue mechanisms; Al_9FeNi particles have been identified to play a major role in ductile fatigue fracture mode.

As it can be seen through this literature review, no study has been realized on multiaxial fatigue behavior of 2618 aluminum alloy and only few deals with uniaxial fatigue loading. And yet, in many appli cations, the parts usually experience multiaxial fatigue loading in ser vice. In this paper, an extended study of fatigue behavior of this alu minum alloy at room temperature is described. Uniaxial tension and torsion fatigue tests have been realized as well as combined tension torsion (with in phase and out of phase conditions). A particular at tention has been paid to the effect of mean stress on the fatigue beha vior. Influence of surface roughness induced by machining has been also investigated. Three axial fatigue tests have been performed too, coupling tensile, torsion and internal pressure loadings. Multiaxial fa tigue results have been analyzed using Crossland generalized fatigue criterion.

2. Material

Fatigue test specimens have been machined in a laminated plate of 2618 T851 aluminum alloy. After laminating process, the plate has been heated at solution treatment temperature (530 ± 5 °C), water quenched and tempered at 190 °C during 20 h. It is then hot worked by tension and finally simultaneously quenched and tempered at 200 °C during some minutes.

The chemical composition of such aluminum alloy is given in table 1. It can be seen, among addition elements, the high level of Iron and Nickel.

The microscopic observation of the microstructure points out a very high level of intermetallic particles of great size, aligned along the la minate direction (see Fig. 1); the mean size of these particles is of 15 µm in L direction (laminate), 12 µm in long transverse direction (width direction of the plate) and 12 µm in short transverse direction (thick direction of the plate). EDX analysis allowed determining chemical nature of these coarse intermetallic particles: it has been found that it was Al_9FeNi intermetallic particles. Finest Al_2Cu hardening particles have been also detected. These observations are in agreement with microstructural observations made by previous researchers [5,7] tem perature [12,17,21,23].

The mechanical characteristics in uniaxial tension and torsion have been determined. The tests have been realized on a multiaxial hydraulic device MTS 809. Specimens have been machined such as longitudinal axis of the specimen was L T direction. Results for both monotonic tests are given in table 2; tensile results were found to be in good agreement with values found in literature [6,13,19,21].

Table 1
Chemical composition (at.%) of 2618 aluminum alloy.

Cu	Zn	Mg	Fe	Si	Mn	Ti	Ni	Al
0.9–1.5	< 0.1	135–2	0.4–0.6	0.2	< 0.15	0.15	0.2–0.6	bal

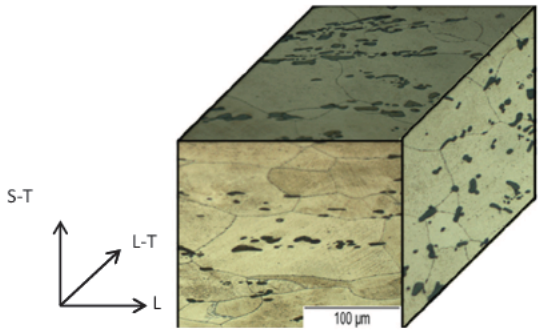

Fig. 1. 3D microstructure of 2618-T851 aluminum alloy (L: laminated direction; L-T: long-transverse direction; S-T: short-transverse direction).

3. Fatigue test specimens and general cyclic loading conditions

As a first step, fatigue tests have been conducted under cyclic ten sion or cyclic torsion, under several stress ratios. For tensile loadings, $R\sigma = 0.1$ has been chosen because it is a conventional stress ratio used in aeronautical fatigue investigations and $R\sigma = -2$ has been chosen in order to extend experimental investigation range and include com pressive mean normal stress. For torsion loadings, $R\tau = -1$ is in vestigated as it is usually used to identify one of the material parameter introduced in most of multiaxial fatigue criteria, and $R\tau = 0.1$has been chosen in order to investigate the sensitivity to mean shear stress of the material. As a previous study on fatigue resistance of 7xxx and 2xxx aluminum alloy pointed out some sensitivity to machined surface roughness [24,25], three levels of surface arithmetic roughness (Ra) have been retained for the characterization: 0.8, 3.2 and 6.3 µm cor responding to general industrial values. In a second time, for a given surface roughness (0.8 µm) fatigue test under combined tension torsion in and out of phase have been conducted and at last some fatigue test under tension torsion internal pressure have been also realized.

The specific geometry of the uniaxial and biaxial (tension torsion) fatigue test specimens is given in Fig. 2. For the loadings involving internal pressure, the geometry of the specimens is given in Fig. 3. Specimens have been turned from prismatic parts extracted in the plate so that axial stress was applied along the L T direction (Fig. 1). (See Fig. 4.)

In the following, for the full and hollow specimens, stresses are expressed in a cylindrical coordinate system as illustrated below for hollow specimens.

All fatigue tests have been realized on a hydraulic MTS 809 multi axial fatigue machine, at the frequency of 10 Hz except for internal pressure fatigue tests which have been conducted at the frequency of 1 Hz.

4. Results and discussion

4.1. Uniaxial fatigue tests

In the following, the graphs represent fatigue data under S N re presentation: the stress amplitude (under tension (σ^{alt}) or torsion (τ^{alt})) is plot in y axis and the number of cycles to failure (*Nf*) on x axis in logarithmic scale.

4.1.1. Influence of surface roughness

Fig. 5 presents fatigue results under tension cyclic loading with a stress ratio $R\sigma$ ($R_\sigma = \frac{\sigma^{min}}{\sigma^{max}}$) of 0.1. As it can be observed, no significant sensitivity to surface roughness can be pointed out. This is rather dif ferent from two other aeronautical aluminum alloys for which a real sensitivity has been observed [24,25].

Fracture surface analysis pointed out the major role of surface in termetallic particles identified to be initiation site of cracks. EDX

Table 2
Monotonic characteristics of 2618-T851 aluminum alloy.

Young modulus E (GPa)	Ultimate tensile stress (MPa)	Tensile yield strength (0, 2%) (MPa)	Compressive yield strength (MPa)	Shear modulus G (GPa)	Shear yield strength (0.2%) (MPa)	Ratio σ_y/τ_y
72	464	438	400	27	260	1.79

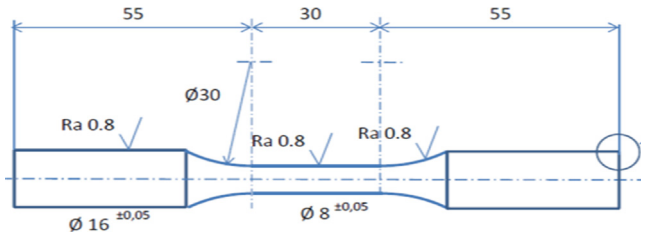

Fig. 2. Geometry of specimens for uniaxial and tension-torsion fatigue test.

analysis pointed out the nature of such particles: Al_9FeNi (Fig. 6). Whatever the stress level is and the surface roughness is, fatigue crack initiate systematically on such kind of particles (Fig. 7).

These particles act as stress concentrators because of their me chanical properties. This phenomenon is well known for aluminium alloys [26,27].

In the case of stress ratio $R\sigma = -2$ (Fig. 8), no more sensitivity can be considered: at 10^6 cycles, the stress decrease is only of 10 MPa, which is lower than observed scatter of the data, which is however greater than the dispersion observed for stress ratio of 0.1. Crack in itiation mechanisms are similar to those observed for a load ratio of 0.1 with Al_9FeNi intermetallic particles as initiation site.

Under uniaxial torsion loadings, no surface roughness sensitivity is observed (Fig. 9); this can be explained by the fact that surface shear stress is aligned with machining (turning) grooves.

Previous studies on aeronautical aluminium alloys pointed out some influence of surface roughness [25,26] so that fatigue life prediction under uniaxial tensile loading based on stress concentration coefficient induced by surface roughness gave good results [27]. These alloys were characterized by an homogeneous repartition of fine strengthening in termetallic particles which were also the initiation site of fatigue cracks. For these alloys, the influence of surface roughness was explained by stress concentration whose intensity was considered of same level than stress concentration due to intermetallic particles so that these two sources could interact. At high stress level, influence of surface roughness disappears because of the larger plastic zone around initia tion site so that stress concentration due to surface roughness does not interact with particles any longer. For the present alloy, such fine mi crostructure is not observed; on the contrary, as it can be seen on Fig. 1, intermetallic particles are so coarse that it becomes obvious that,

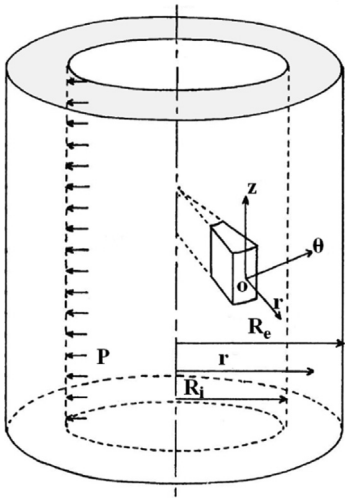

Fig. 4. Cylindrical coordinates system used to express internal pressure loading.

whatever the stress level is, stress concentration due to these particles is predominant compared to stress concentration due to surface rough ness.

4.1.2. Influence of stress ratio

Influence of tensile and torsion stress ratio on fatigue lifetime has been investigated for a given surface roughness of 0.8 µm. Concerning stress ratio effect for uniaxial tensile cyclic loadings (Fig. 10); the re sults are in agreement with expected results in this fatigue regime: the deleterious influence of positive tensile stress on fatigue resistance can be observed. This experimental result has been largely presented through literature and most fatigue criteria take into account some mechanical quantity in order to reproduce this influence.

Under torsion cyclic loadings, sensitivity to shear mean stress is also observed even if maximum shear stress is less than shear yield stress (Fig. 11). Same influence has been observed by Zhang [28] for Al2A12 T4 and Gates for Al 2024 T3 [29]. It clearly appears that this influence decreases for low shear stress amplitude. This is why most of the multiaxial fatigue criteria, developed for fatigue limit, do not take into account this influence. This obviously must be considered carefully

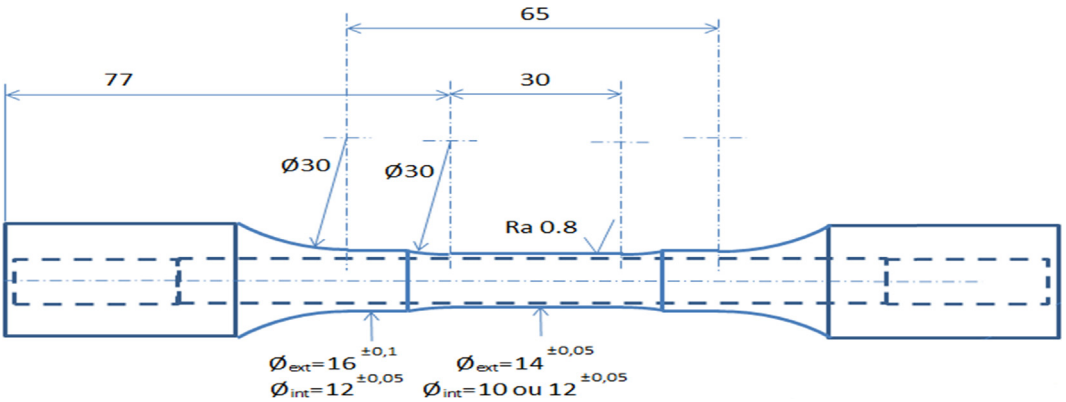

Fig. 3. Geometry of specimens for combined loading fatigue test with internal pressure.

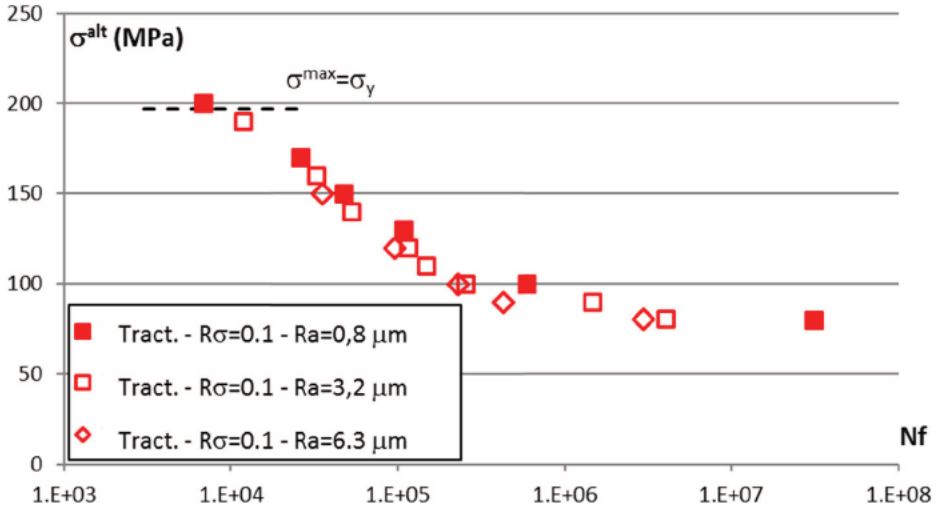

Fig. 5. Fatigue results in tensile cyclic loading - Stress ratio Rσ = 0.1 – Effect of surface roughness.

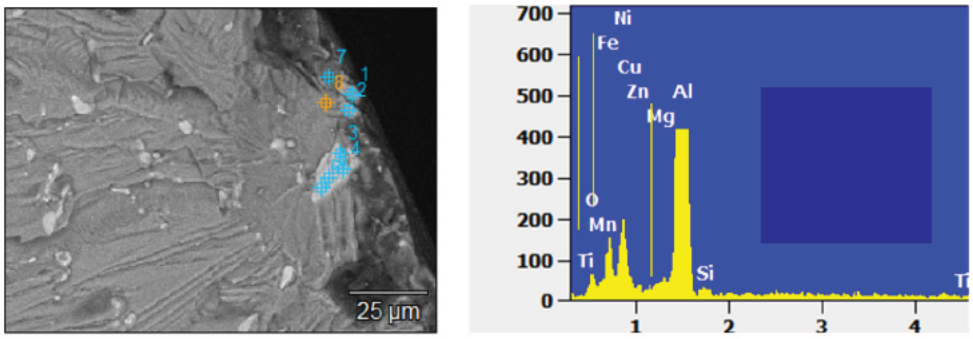

	C-K	O-K	Mg-K	Al-K	Si-K	Ti-K	Mn-K	Fe-K	Ni-K	Cu-K	Zn-K
At%	9.18	5.91	0.34	68.79	0.61	0.00	0.14	6.88	6.52	1.28	0.35

Fig. 6. EDX analysis of intermetallic particle at the fatigue crack initiation site.

when using such criteria for limited fatigue lifetime.

4.2. Combined tensile torsion in and out of phase tests

Two load cases of combined tensile torsion loading have been ap plied on specimens with same roughness level (R_a = 0,8µm); each case is characterized by the stress ratio Rσ on each axis and the ratio be tween the alternating shear stress and the alternating normal stress called the stress amplitude ratio $\lambda = \frac{\tau^{alt}}{\sigma^{alt}}$ (denoted $\frac{t}{s}$ in Fig. 12). For each load case, two fatigue tests have been realized: one with in phase conditions and the other with out of phase conditions with a phase shift of 90°. Table 3 resumes all the bi axial tests conditions and corre sponding fatigue life.

Fig. 12 shows results obtained under a same Von Mises equivalent alternate stress with two biaxial stress ratios (0.47 and 2.75); for each loading direction, the stress ratio on each axe is equal to −1 (purely alternated). As it can be seen:

for a same Von Mises equivalent alternate stress (≃192 MPa in that case), fatigue life depends on biaxial stress ratio: the higher the biaxial stress ratio is, the higher fatigue life; that means that for a given level of alternate equivalent stress, tensile stress is more det rimental than shear stress; let's remark that it has been found that fatigue life reduces with the increase of torsional stress participation for 2017, 2024, 7075 and 6068 aluminum alloys [30 32].
fatigue life seems not to be sensitive to the phase shift, whatever the biaxial stress ratio is: it is observed that, for each case of biaxial stress ratio, the fatigue life in phase and out of phase conditions are similar; same kind of results have been found for 2A12 aluminum alloy [33] and opposite results have been found for 2007 aluminum alloy [34].

Fig. 13 shows results obtained under the same biaxial stress ratio λ (0.47) but with mean stress introduced in tensile or torsion direction. It appears that a positive mean tensile stress (empty diamond plot) leads to an important reduction of fatigue life compared zero mean tensile stress (empty round plot). Same observation can be made concerning the influence of mean shear stress (full diamond and round plots) even if the reduction of fatigue life is lower. These results are in agreement with the relative influence of tensile mean stress and shear men stress which has been previously observed.

At last it must be noted that fracture surface observations revealed that crack initiation occurs, as for uniaxial loading, on coarse inter metallic particles on the outer surface.

4.3. Combined tensile torsion internal pressure loadings

Only few multiaxial fatigue tests have been conducted under mul tiaxial cyclic loading including internal pressure. Results are given in Table 4. Tests have been conducted with a stress ratio Rσ of 0.1 on each loading axis. No phase shift has been introduced. Direct commentaries on these results are impossible; it is necessary to use some multiaxial fatigue criteria in order to compare these experimental results to some fatigue life predictions. Whatever the loading, coarse intermetallic

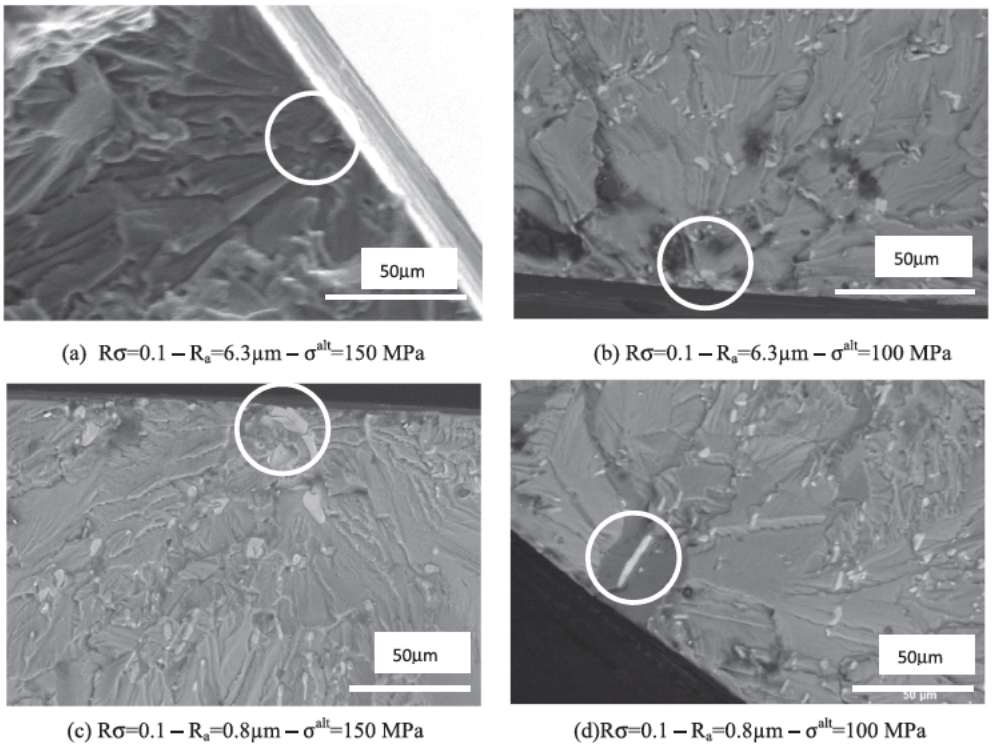

(a) Rσ=0.1 – R_a=6.3µm – σ^{alt}=150 MPa (b) Rσ=0.1 – R_a=6.3µm – σ^{alt}=100 MPa

(c) Rσ=0.1 – R_a=0.8µm – σ^{alt}=150 MPa (d)Rσ=0.1 – R_a=0.8µm – σ^{alt}=100 MPa

Fig. 7. Fatigue fracture observation – Stress ratio 0.1 – intermetallic particles at crack initiation sites (a) high roughness and high stress level – (b) high roughness and low stress level (c) low roughness and high stress level – (d) low roughness and low stress level.

particles were found at initiation sites.

5. Generalized Crossland multiaxial fatigue criterion

In order to analyze the multiaxial fatigue behavior of 2618 T851 aluminum alloy, Crossland criterion has been selected because of its simplicity. Let's recall that Crossland criterion expresses a limitation of a fatigue equivalent stress which introduces both Von Mises equivalent alternate stress $\sigma^{alt}_{eq,VM}$ and maximal hydrostatic pressure P^{max} through a linear combination:

$$\sigma^{alt}_{eq,VM} + \alpha \bullet P^{max} \leq \beta \quad (1)$$

where α and β represent two material parameters to be identified using two fatigue limits, for example in fully reversed tensile and torsion loadings.

In order to make fatigue life predictions, it is necessary to replace the two parameters α and β by two *Nf* depending functions; then expression (1) becomes:

$$\sigma^{alt}_{eq,VM} + \alpha(Nf) \bullet P^{max} \leq \beta(Nf) \quad (2)$$

where $\alpha(Nf)$ and $\beta(Nf)$ represent two material parameter function to be identified using two fatigue curves, for example in fully reversed tensile and torsion loadings.

Fig. 14 illustrates the result of material characterization of 2618 T851 aluminum alloy using three fatigue curves: the uniaxial tensile fatigue curves for the two stress ratio −2 and 0.1, and the fully reversed torsion fatigue curve. The so called $\sigma_{eq,CR}$ (Crossland equivalent fatigue stress), on the vertical graduation, is equal to:

$$\sigma_{eq,CR} = \sigma^{alt}_{eq,VM} + \alpha \bullet P^{max} \quad (3)$$

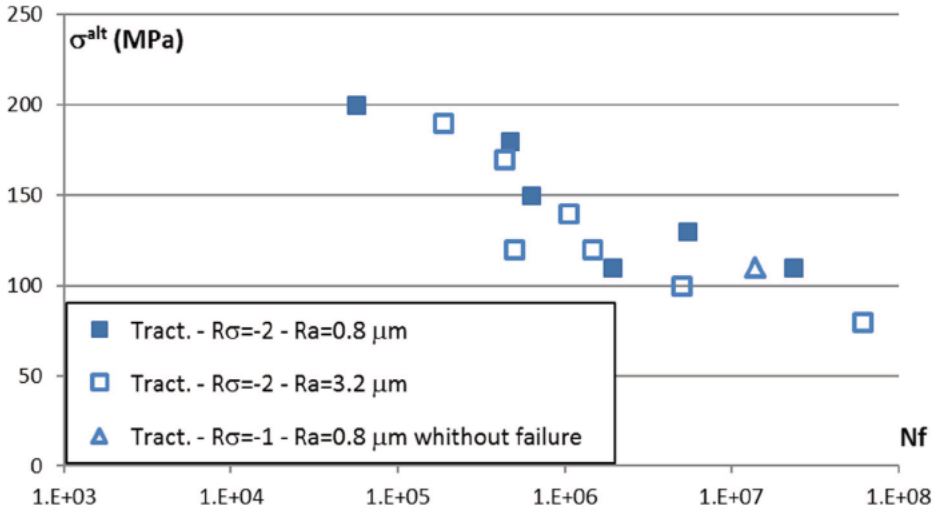

Fig. 8. Fatigue results in tensile cyclic loading – Stress ratio Rσ = 2 – Effect of surface roughness.

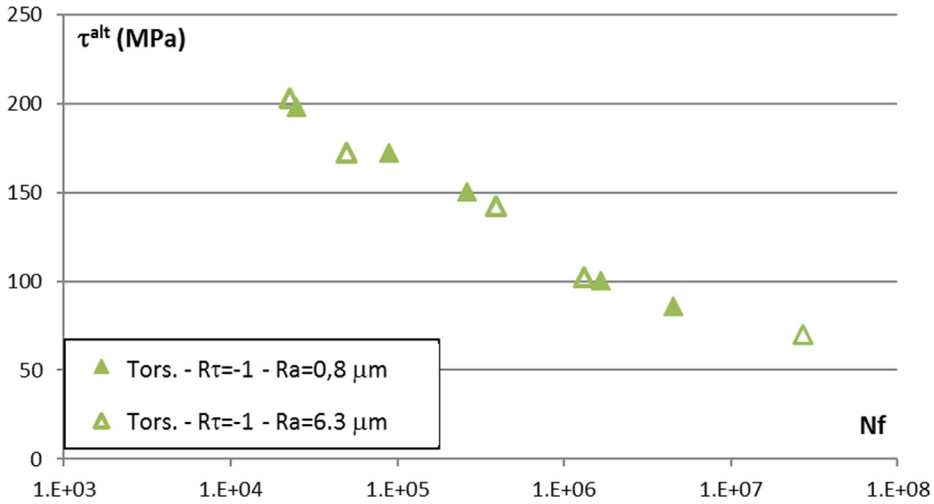

Fig. 9. Fatigue results in torsion cyclic loading – Stress ratio Rτ = 1 – Effect of surface roughness.

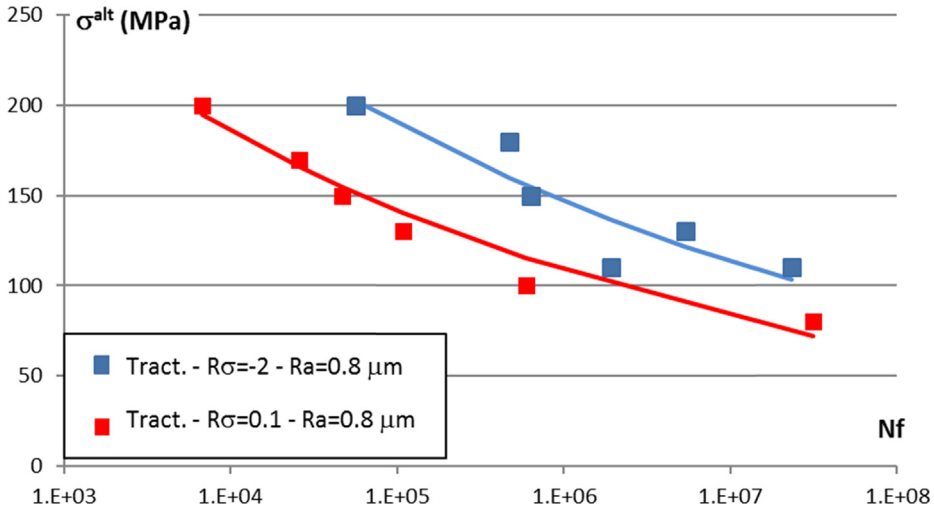

Fig. 10. Fatigue results in tensile cyclic loading – Ra = 0.8 µm – Effect of stress ratio Rs.

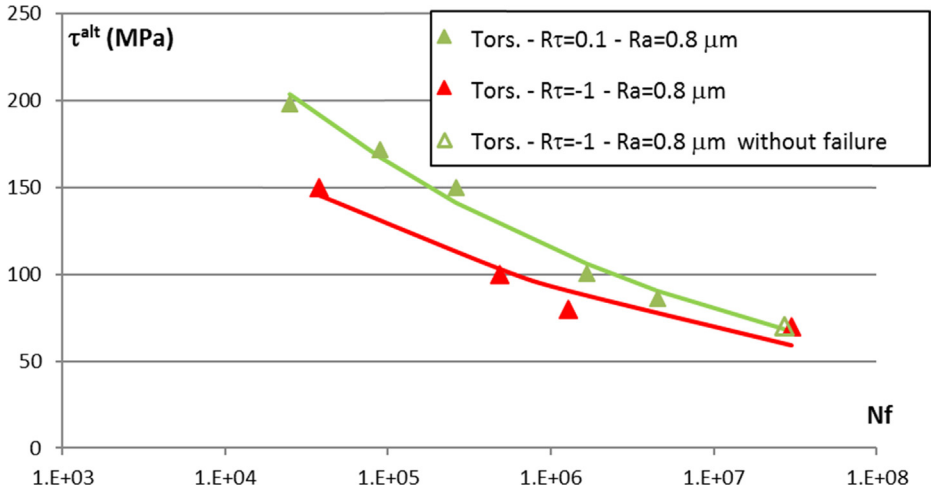

Fig. 11. Fatigue results in torsion cyclic loading – Ra = 0.8 µm – Effect of stress ratio Rs.

The fatigue curve $\beta(Nf)$ that fit the chosen experimental data can be considered as the referenced S N curve for the studied alloy. The al ternate stress standard deviation is of 20.7 MPa

Using this material characterization of 2618 T851 aluminum alloy, fatigue results under combined tensile torsion loading (in or out of phase) and under three axes multiaxial loading can be represented in the Crossland S N diagram (Figs. 15 and 16). Plot under the mean β curve mean that the calculated fatigue equivalent stress is lower than

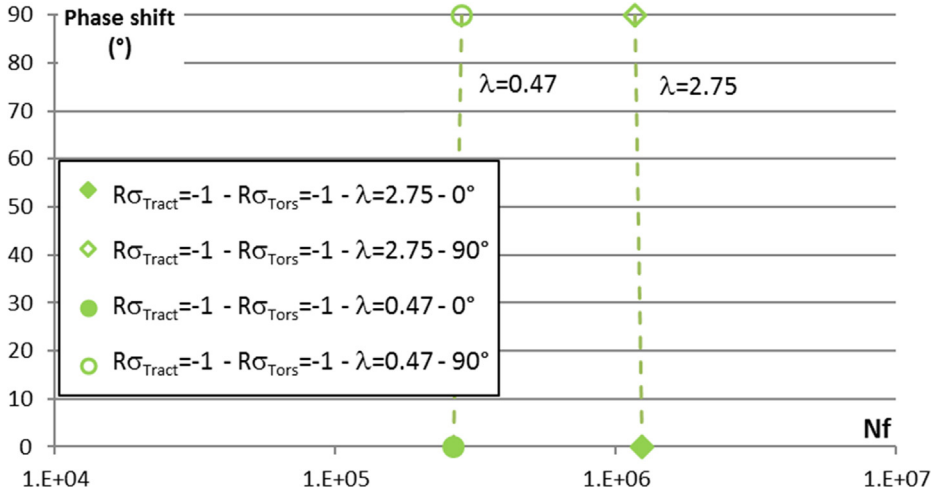

Fig. 12. Fatigue results for tensile-torsion cyclic loading – Effect of in or out of phase for two values of biaxial stress ratio λ.

Table 3
Fatigue tests results under bi-axial tension-torsion.

Tension		Torsion				
σ_{zz}^{alt}	Rσ	$\sigma_{z\theta}^{alt}$	Rτ	Phase shift (°)	λ	Nf
40	1	110	1	0	2.75	1.243×10^6
40	1	110	1	90	2.75	1.17×10^6
150	1	70	1	0	0.47	2.64×10^5
150	1	70	1	90	0.47	2.81×10^5
150	1	100	0.1	90	0.67	7.425×10^4
150	1	70	0.1	0	0.47	9.948×10^4
150	0,1	70	1	90	0.47	3.356×10^4
137	1	97	1	0	0.7	1.364×10^6
95	1	193	1	0	2.03	2.05×10^4

Table 4
Fatigue tests results under combined tensile-torsion-internal pressure.

Tensile	Torsion	Internal pressure	Nf
σ_{zz}^{alt}	$\sigma_{z\theta}^{alt}$	$\sigma_{\theta\theta}^{alt}$	cycles
100	0	20.83	1.33×10^5
90	0	18.75	2.58×10^5
0	90	18.75	1.95×10^5
0	69	14.4	1.467×10^6
100	100	20.83	1.94×10^4
69	69	14.4	1.14×10^5
50	50	10.4	$> 10^6$

experimental value corresponding to the same number of cycles to failure, or an another way, the corresponding fatigue life prediction is higher than experimental one so that prediction is not conservative. One can observe a large scatter of predictions around the mean β curve. In particular, Crossland criterion is not able to reproduce the effect of shear mean stress (red triangular plots in Fig. 15). However, one can remark that some results for combined tensile torsion loadings are above the mean β curve, which means conservative fatigue life predictions. For combined tensile and/or torsion and internal pressure, results are quite all below the underlying dashed β curve which corresponds to thirds of the mean lifetime (Fig. 16); for such loadings, Crossland criterion is not able to give any good fatigue life predictions.

6. Conclusions

An exhaustive fatigue study of 2618 T851 aluminum alloy has been realized; 66 fatigue tests have been conducted under various kinds of loading: uniaxial tensile loading for 2 stress ratio (−2 and 0.1); torsional loading under two shear stress ratio (1 and 0.1); combined tensile torsion loadings under in or out of phase conditions and different stress ratio (−1 and 0.1); combined tensile torsion internal pressure on tubular specimens. Effect of surface roughness induced by machining on uniaxial fatigue behavior has also been investigated. It has been observed that:

No significant influence of machined surface roughness on fatigue resistance has been clearly observed for tensile loadings regardless of the stress ratio; for torsion loadings, it is obvious that there is no influence.

Fatigue behavior resistance is sensitive to mean tensile stress as well

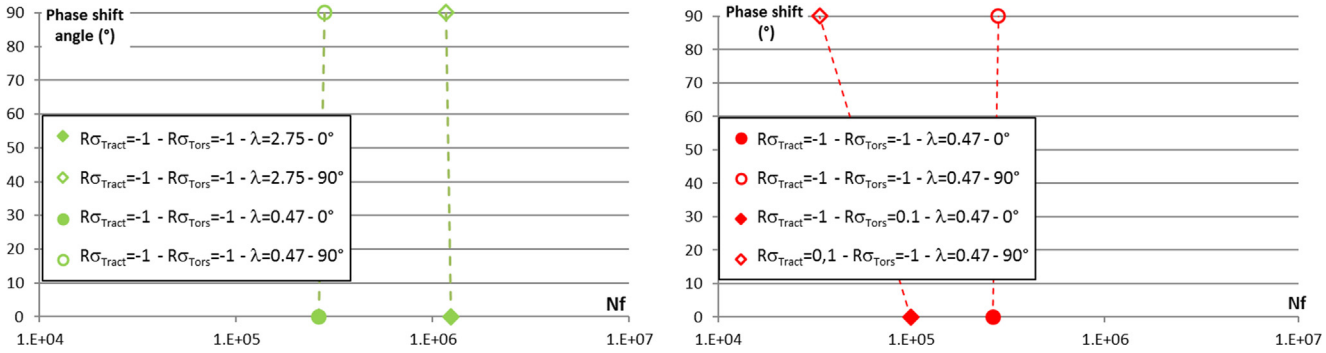

Fig. 13. Fatigue results in tensile-torsion cyclic loading – Effect of in or out of phase with mean normal stress or mean shear stress.

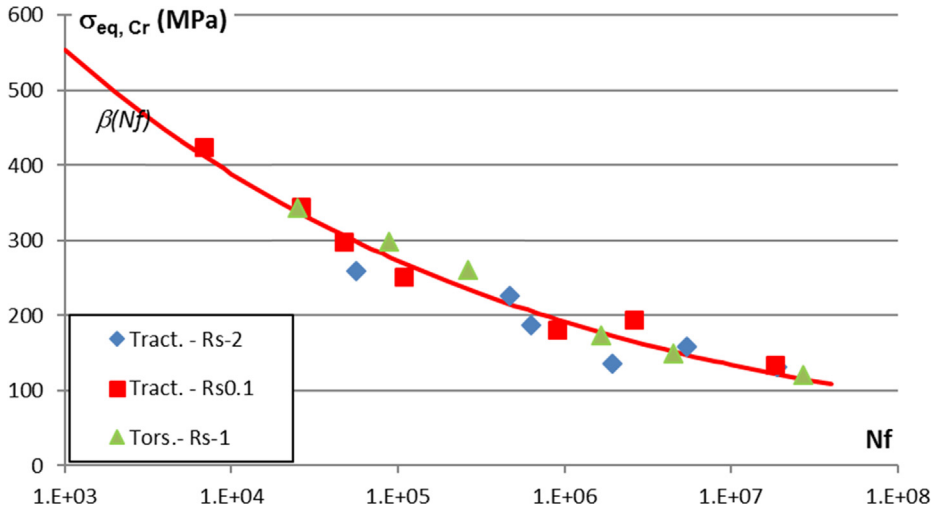

Fig. 14. Crossland criterion characterization for 2618-T851 aluminum alloy.

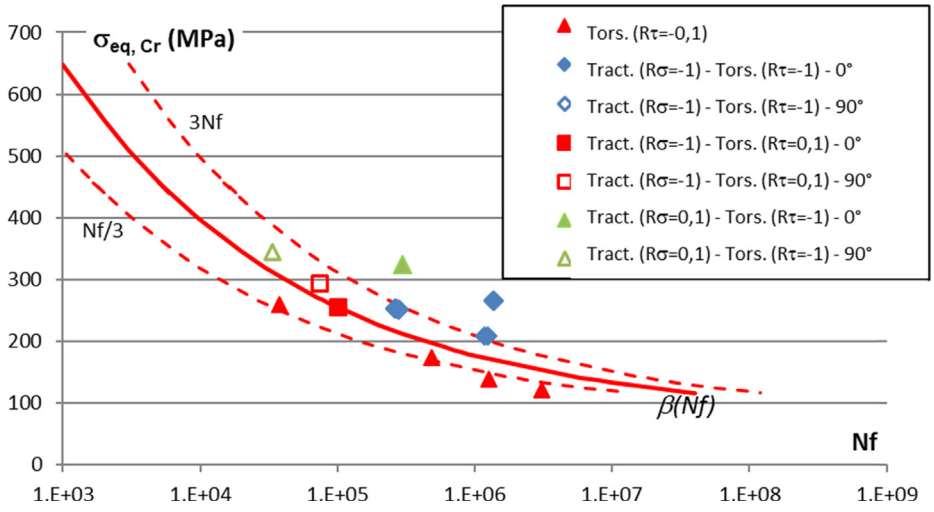

Fig. 15. Results for combined tensile-torsion loadings (in and out of phase) for Al-2618-T851 in Crossland's diagram.

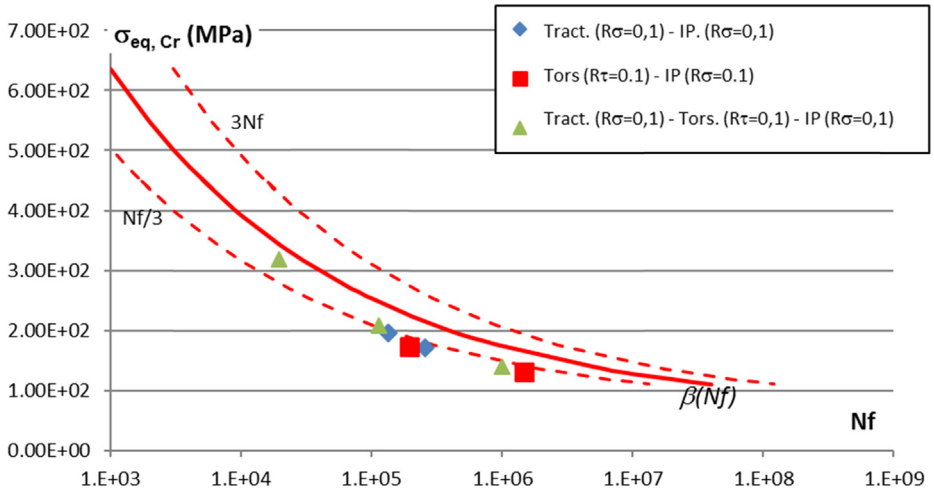

Fig. 16. Results for combined tensile-torsion-internal pressure loadings for Al-2618-T851 in Crossland diagram.

as mean shear stress.

Under combined tensile torsion loadings, the influence of phase shift is negligible.

For all loadings, fatigue cracks initiate systematically on Al_9FeNi coarse intermetallic particles

Crossland generalized fatigue criterion is not able to reproduce correctly the experimental results obtained with multiaxial fatigue loadings, especially when mean shear stress and internal pressure is

introduced.

It seems obvious that the specific microstructure of 2618 aluminum alloy, characterized by a very high density of Al_9FeNi coarse particles disseminated in grains highly influence the fatigue behavior. Compared to 2214 or 7050 aluminium alloys, such microstructure annihilates surface roughness effect. Perhaps 2618 microstructure could also ex plain the great influence of mean shear stress on fatigue resistance; this must be investigated more precisely by looking carefully at the me chanisms involved in the fatigue damage. Because of this particular sensitivity, any multiaxial fatigue criteria which does not include some mechanical terms relative to mean shear stress, such as Crossland used in this paper, will not be able to provide good fatigue life predictions for loading conditions including mean shear stress. Research work on a new criterion, based on Macha Lagoda bi axial fatigue criterion, in cluding shear mean stress, is currently in progress.

Declaration of Competing Interest

The authors declared that there is no conflict of interest.

Acknowledgements

Special thanks are given to Université Paul Sabatier (Toulouse) for financial support of this research study and to IRT M2P, in particular Joffrey Tardelli (IRT M2P), Benjamin Mouls (IRT M2P), Cédric Marchetto (IRT M2P) and Aimé Ramakistin (INEOSURF).

References

[1] Doyle WM. The development of Hiduminium-RR58 aluminium alloy: the background to the choice of the main structural material for Concorde. Aircr Eng Aerosp Technol 1969;41:11–4.
[2] Williams JC, Starke Jr EA. Progress in structural materials for aerospace systems. Acta Mater 2003;51:5775–99.
[3] Romanowski CA. The annealing characteristics of Hiduminium RR58 PhD thesis University of Surrey; 1981.
[4] Oguacha I, Yannacopoulos S. The structure of AlxFeNi phase in Al-cu-mg-Fe-Ni alloy ‘AA2618). Mater Sci 1996;9:615–23.
[5] Ozbek I. A study on the re-solution heat treatment of AA2618 aluminium alloy. Mater Charact 2007;58:312–7.
[6] Wang J, yi D, Su X, Yin F. Influence of deformation ageing treatment on microstructure and properties of aluminium alloy 2618. Mater Charact 2008;65:965–8.
[7] Novy F, Janecek M, Kral R. Microstructure changes in 2618 aluminium alloy during ageing and creep. J Alloy Compounds 2009;487:146–51.
[8] Chobaut N, Carron D, Drezet JM. characterization of precipitation upon cooling of an AA2618 Al-Cu-Mg alloy. J. Alloys Compounds 2016;654:56–62.
[9] Lumm JA. Mechanical properties of 2618 aluminum alloy. North American Aviantion, Inc., Technical report AFML-TR-66-238; 1966.
[10] Doyle WM. Development of Hidunium-RR-58 structural aluminium alloy used on. Concorde 1969:2016–220.
[11] Royster DM. Tensile properties and creep strength of three aluminium alloys exposed up to 25000 hours at 200° to 400°F, Langley research Center. NASA Scientific and Technical Publications, NASA TN D-5010; 1969.
[12] Leng Y, Porr Jr WC, Gangloff RP. Tensile deformation of 2618 and Al-Fe-Si-V aluminium alloy at elevated temperatures. Scrip Metallurg Mater 1990;24:2163–8.
[13] Khalil O, Lang KH. Influence of microstructure on the quasistatic and low cycle fatigue behavior of an AA2618 aluminium alloy. Proc Eng 2011;10:1339–47.
[14] Kazanjian SM, Wang N, Strarke Jr. EA. Creep behaviour and microstructural stability of al-Cu-Mg-Ag and Al-Cu-Li-Mg-Ag alloys. Mater. Sc. Eng. 1997;A234–236:571–4.
[15] Cavaliere P. Hot and warm forming of 2618 aluminium alloy. J Light Met 2002;2:247–52.
[16] Bueno LO, Bell RL. Anelastic creep behavior of RR-58 aluminium alloy at 180°c: phenomenological aspects and analysis based on the unbowing of dislocation segments. Mater Sci Eng A 2005:72–8.
[17] Elgallad EM, Shen P, zhang Z, Chen XG. Effects of heat treatment on the microstructure and mechanical properties of AA2618 DC cast alloy. Mater Des 2014;61:133–40.
[18] Robin C, Pluvinage G. Fatigue threshold in a 2618A aluminium alloy. Fat. Eng. Mat Struct 1980;3:147–57.
[19] Bathias C. Influence of various parameters on the determination of the fatigue crack arrest threshold. Fat Eng Mater Struct 1981;4:1–13.
[20] Gariboldi E, Ripamonti D, Signorelli L, Vimercati G, Casaro F. Fracture toughness and microstructure in AA 2xxx aluminium alloys. Metall Sci Technol 2007;25:3–11.
[21] Aghaie-Khafri M, Zargaran A. Low-cycle fatigue behavior of AA2618-T61 forged disk. Mater Des 2010;31:40104–4109.
[22] Zamarripa AS, Pinna C, Brown MW, Guerruro MP, Castillo Morales M, Beber-Solano TP. Indentification of modes of fracture in a 2618–T6 aluminium alloy using stereophotgrammetry. Mater Charact 2011;62:1141–50.
[23] Moreira MF. Failure analysis in aluminium turbocharger wheels. Eng. Failure Anal 2016;6:108–18.
[24] Suraratchaï M, Limido J, Mabru C. Modelling the influence of machined surface roughness on the fatigue life of aluminium alloy. Int. J. Fatig 2008;30:2119–26.
[25] Shahzad M, Chaussumier M, Chieragatty R, Mabru C, Rézaï-Aria F. Influence of surface treatments on fatigue life of Al 7010 alloy. J. Mater Process Tech 2010;210:1821–6.
[26] Shahzad M, Chaussumier M, Chieragatti R, Mabru C, Rezaï-Aria F. Effect of sealed anodic film on fatigue performance of 2214–T6 aluminium alloy. Surf Coat Technol 2012;206:2733–9.
[27] Chaussumier M, Shahzad M, Mabru C, Chieragatti R, Rezaï-Aria F. A predictive fatigue life model for anodized 7050 aluminium alloy. Int J Fat 2013;48:205–13.
[28] Zhang J, Xiao Q, Shi X, Fei B. Effect of mean shear stress on torsion fatigue failure behavior of 2A12-T4 aluminium alloy. Int J Fat 2014;67:173–82.
[29] Gates NR, Fatemi A. On the consideration of normal and shear stress interaction in multiaxial fatigue damage analysis. Int J Fat 2017;100:322–36.
[30] Lagoda T, Ogonowski P. Fatigue life of AlCu4Mg1 aluminium alloy under constant-amplitude in- and out-of-phase bending with torsion. Proced. of the 7th Inter Conf on Biax/Multiax Fatigue and Fracture. Berlin: DVM; 2004. p. 197–202.
[31] Niesłony A, Lagoda T, Walat K, Kurek M. Multiaxial fatigue behaviour of AA6068 and AA2017A aluminium alloys under in-phase bending with torsion loading condition. Mater Werkstofftech 2014;45.
[32] Neerukatti RK, Datta S, Chattopadhyay A, Iyyer N, Phan N. Fatigue crack propagation under in-phase and out-of-phase biaxial loading. Fatig Fract Eng Mater Struct 2017:1–13.
[33] Zhang J, Shi X, Bao R, Fei B. Tension–torsion high-cycle fatigue failure analysis of 2A12-T4 aluminum alloy with different stress ratios. Int J Fat 2011;33:1066–74.
[34] Uhríčik M, Kopas P, Palček P, Hurtalová L. Determine the fatigue lifetime for aluminium alloy EN AW 2007.T3 during cyclic bending-torsion loading under in-and-out of phase shift $\varphi = 0°$ and $\varphi = 90°$ using selected fatigue criteria. Sci Proc XIII Int Congr “Mach Technol Mater” 2016.